

# Evaluating the Intrinsic Cysteine Redox-Dependent States of the A-Chain of Human Insulin Using NMR Spectroscopy, Quantum Chemical Calculations, and Mass Spectrometry

Alok K. Sharma,<sup>†</sup> Yan Ling,<sup>‡</sup> Allison B. Greer,<sup>§</sup> David A. Hafler,<sup>§</sup> Sally C. Kent,<sup>§</sup> Yong Zhang,<sup>\*,‡</sup> and Alan C. Rigby<sup>\*,†</sup>

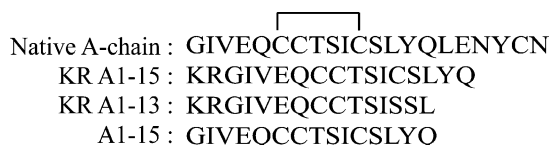
Center for Vascular Biology Research, Division of Molecular and Vascular Medicine, Department of Medicine, Beth Israel Deaconess Medical Center, Harvard Medical School, Boston, Massachusetts 02215, Department of Chemistry and Biochemistry, The University of Southern Mississippi, 118 College Drive #5043, Hattiesburg, Mississippi 39406-0001, and Center for Neurologic Diseases, Brigham and Women's Hospital, Harvard Medical School, Boston, Massachusetts 02115

Received: September 9, 2009; Revised Manuscript Received: November 6, 2009

Previous functional studies have proposed that solution-phase loading of human insulin A-chain peptides into cell surface Class II molecules may be limited by the redox state of intrinsic cysteine residues within the A-chain peptide. T cell functional studies of a human insulin A-chain analogue (KR A1–15) comprised of residues 1–15 of the A-chain peptide as well as an amino-terminal lysine-arginine extension have been carried out in a reducing environment. These data suggest that free thiol moieties within this peptide may participate in major histocompatibility complex (MHC) II/peptide interactions. Two-dimensional <sup>1</sup>H NMR spectroscopy data partnered with quantum chemical calculations identified that KR A1–15 exists in conformational flux sampling heterogeneous redox-dependent conformations including: one reduced and two oxidized states. These findings were further supported by mass spectrometry analysis of this peptide that confirmed the presence of a redox state dependent conformational equilibrium. Interestingly, the presence of a free thiol (<sup>1</sup>H<sup>γ</sup>) resonance for cysteine 8 in the oxidized state supports the existence of the third redox-dependent conformation represented as a mixed disulfide conformation. We believe these data support the presence of a redox-dependent mechanism for regulating the activity of human insulin and provide a better understanding of redox chemistry that may be extended to other protein systems.

## Introduction

Human insulin has become a therapeutically important target for human diabetes mellitus.<sup>1</sup> Insulin is comprised of two chains, an A-chain and a B-chain, which are comprised of 21 and 30 residues, respectively. Endogenously, these two chains are linked via two intermolecular disulfide bonds between cysteine residues (Cys) at position 7 from the A- and B-chains (A7, B7) and Cys20 and Cys19 from the A-chain and B-chain (A20, B19), respectively. Importantly, it is believed that an intramolecular disulfide bond between Cys residues at positions 6 and 11 in the A-chain peptide is important for activity.<sup>2</sup> The isolated A-chain of insulin possesses sufficient structural information to form the native/active conformation,<sup>3</sup> as observed in studies demonstrating that the A-chain functions as a T cell epitope. Previous studies by our group and others have identified and reported that insulin A-chain peptides, A1–15, KR A1–15 (native peptide with N-terminal lysine (Lys), arginine (Arg) extension), as well as a KR A1–11 variant and/or the A1–12 (a C-terminal truncated peptide) variant illustrated in Figure 1, are functionally important.<sup>4</sup> The presence of three Cys residues in these peptides, each of which is capable of forming intra- and/or intermolecular disulfide bonds, represents a potential barrier for solution-phase loading of these peptides into the cell surface Class II major histocompatibility complex (MHC).<sup>4b–d</sup>


  
Native A-chain : GIVEQCCTSICS<sup>—</sup>LYQLENYCN
   
KR A1-15 : KRGIVEQCCTSICS<sup>—</sup>LYQ
   
KR A1-13 : KRGIVEQCCTSISSL
   
A1-15 : GIVEQCCTSICS<sup>—</sup>LYQ

**Figure 1.** Primary sequence of human insulin A-chain peptide and functional analogues.

Early studies with the bovine insulin A-chain epitope, A1–14 by Jensen et al., demonstrated the presence of a thiol-dependent insulin determinant that was requisite for immunogenicity.<sup>5</sup> However, in a recent study of the A-chain epitope KR A1–13 (Figure 1), Mannering et al. demonstrated that the function of a naturally processed A-chain epitope was dependent on the formation of a vicinal disulfide bond between adjacent Cys residues (Cys6–Cys7) and that removal of this intramolecular disulfide bond abrogates T cell stimulation.<sup>4b</sup> These diametric conclusions for the insulin A-chain peptides prompted us to study the “redox state” and/or conformational role of each Cys residue in the A-chain peptide, KR A1–15. Here, we report data obtained from two-dimensional (2D) nuclear magnetic resonance (NMR) spectroscopy, mass spectrometry, and computational quantum chemical investigations on this peptide. Taken together, these data support the coexistence of three Cys-dependent redox states, a phenomenon discernible at the atomic level by NMR spectroscopy. These data represent a novel, redox-dependent mechanism for the action of insulin that we believe may have applications to other proteins susceptible to redox chemistry.

\* Corresponding author. E-mail: arigby@bidmc.harvard.edu (A.C.R.); yong.zhang@usm.edu (Y.Z.).

<sup>†</sup> Beth Israel Deaconess Medical Center, Harvard Medical School.

<sup>‡</sup> The University of Southern Mississippi.

<sup>§</sup> Brigham and Women's Hospital, Harvard Medical School.

## Experimental Methods

Human insulin A-chain peptide KR A1–15 (KRGIVEQC-CTSICSLYQ) was synthesized using standard Fmoc-chemistry and purified using reverse phase HPLC, as described previously.<sup>6</sup> The purified peptide was lyophilized and used for NMR sample preparation as described (see Supporting Information for details).

NMR experiments were performed on a Bruker Avance 600 MHz spectrometer equipped with a triple resonance (*z*-axis) pulsed field gradient probe. Two-dimensional <sup>1</sup>H–<sup>1</sup>H DQF-COSY and TOCSY spectra with a Dipsi2rc spin-lock<sup>7</sup> of 50 and/or 70 ms were acquired. Rotating Frame Nuclear Overhauser Spectroscopy (ROESY) data with a 200 and 400 ms spin-lock mixing time were collected for both peptides, while NOESY data at two different mixing times (150 and 300 ms) were collected to ensure sufficient magnetization transfer and optimize the NOE signal. Natural abundance <sup>1</sup>H–<sup>13</sup>C constant time HSQC data<sup>8</sup> were also recorded for both the peptides with 1024 and 200 data points in the direct and indirect dimensions, respectively, to complete and/or verify resonance assignments. All NMR data were acquired in the phase-sensitive mode with the time proportional phase increments (TPPI) mode for quadrature detection in the *t*<sub>1</sub> dimension. Water suppression was achieved using the WATERGATE pulse sequence. The digital resolution in the direct dimension was 3.8 Hz/pt for all 2D data acquisitions. The sample temperature was maintained at 15 °C during all 2D experiments.

NMR data were processed on an Intel PC workstation running Red Hat Linux 7.3 using the NMRPipe/NMRDraw<sup>9</sup> processing software. Both the direct and indirect detected time domain data for the 2D experiments were processed by applying a 90° phase-shifted squared sinebell or a Gaussian filter with a line-broadening weight function of 15 Hz. Data sets were zero filled once in each dimension prior to Fourier transformation. Frequency discrimination in the indirect dimensions was achieved using the States-TPPI mode of quadrature detection. All chemical shifts were referenced with respect to the residual DMSO-*d*<sub>6</sub> proton at 2.50 ppm. The NMR spectra were visualized and assignments completed using ANSIG.<sup>10</sup>

For mass investigation, the KR A1–15 peptide was diluted 1:100 into a solution of the standard peptide MALDI matrix CHCA (stock solution was at 5.0 mg/mL). Peptide samples (with or without DTT) were spotted directly onto the 4800 OptiTOF metal target plate. MALDI-TOF MS analysis was used to determine the *m/z* ratio of the peptide(s) present on an AB/MDS Sciex 4800 Plus MALDI TOF/TOF Analyzer (Applied Biosystems). The instrument was operated in the positive ion mode at 2 kV. External calibration was performed on the same target plate at the time of the analysis using the five-peptide 4700 Cal mix (Applied Biosystems). Samples spotted onto MALDI plates are dried, and the molecule composition of the peptides is fixed at that time point. The data are collected as total ion current (TIC) from 500 laser shots, and the time scale is on the order of milliseconds (ms). These conditions prevent interconversion of the peptides in the MALDI data.

To evaluate the presence of heterogeneous conformational states of cysteine residues in the KR A1–15 peptide, *ab initio* quantum chemical calculations were performed using a density functional theory method, B3LYP,<sup>11</sup> with a large basis set 6-311++G(2d,2p) and the gauge independent atomic orbitals (GIAO) method<sup>12</sup> in Gaussian 03,<sup>13</sup> a computational approach that has been used previously for studying other peptides.<sup>14</sup> A self-consistent reaction field model was also included as described previously<sup>14a</sup> to simulate the general effect of the bulk protein environment, which was found to effectively improve

the prediction accuracy. The predicted <sup>1</sup>H NMR chemical shift ( $\delta$ ) is derived from the quantum chemically calculated chemical shielding ( $\sigma$ ) with respect to that of TMS ( $\sigma_{\text{TMS}}$ ), namely,  $\delta = \sigma_{\text{TMS}} - \sigma$ , in which the calculated <sup>1</sup>H NMR chemical shielding of TMS using the same quantum chemical method is 31.35 ppm.

## Results and Discussion

The naturally processed A-chain epitope (KR A1–15) stimulates T cell clones in a reduced environment (Supporting Information and Figure S1). To evaluate the intrinsic conformational flux exhibited by Cys residues (Cys8, Cys9, and Cys13) in KR A1–15 and to understand the importance of a reduced environment [presence of dithiothreitol (DTT) in functional studies] we collected 2D homonuclear and 2D heteronuclear <sup>13</sup>C NMR data in the absence and presence of DTT.

The NMR spectra identified spectrally resolved resonances for each amino acid, which we used to complete the assignment of the peptide (see Supporting Information, Figure S2 and Table S1 for details).<sup>15</sup> Upon analyzing the <sup>1</sup>H–<sup>1</sup>H 2D TOCSY and NOESY fingerprint spectra collected in the absence of DTT, we determined that the three Cys spin systems in KR A1–15 sampled more than a single conformational state. Three unique conformations were unambiguously observed for the Cys8 and Cys13 residue: one major and two minor conformations in a ratio of 77%:13%:10% ( $\pm 3\%$ ) on the basis of crosspeak intensities observed in homonuclear spectra. For the Cys9 residue, one major and one minor conformational state were observed in a ratio 93%:7% ( $\pm 3\%$ ), respectively. These Cys residues were observed in a redox-dependent conformational equilibrium (Figure 2).

The unique <sup>1</sup>H <sup>$\beta$</sup>  resonance chemical shifts of the reduced and oxidized states were identified for each Cys residue.<sup>16</sup> The major conformation has <sup>1</sup>H <sup>$\beta$</sup>  chemical shifts that are representative of a reduced peptide conformation, i.e., free thiol (–S–H state) for all three Cys residues (Figure 2A and Table S1 in the Supporting Information), while minor conformations for Cys8, Cys9, and Cys13 all possess <sup>1</sup>H <sup>$\beta$</sup>  chemical shifts representative of Cys residues in an oxidized (–S–S–) state (Figure 2B and Table S1 in the Supporting Information). The population ratio between two minor oxidized conformations of Cys8 and Cys13 is 0.55:0.45 ( $\pm 0.05$ ) (Figure 2B).

These homonuclear assignments were further supported by natural abundance <sup>1</sup>H–<sup>13</sup>C 2D heteronuclear single quantum correlation (HSQC) data that were acquired in the absence of DTT (Figure S3 in the Supporting Information and Figure 2D). These spectra illustrate the presence of Cys residue <sup>13</sup>C <sup>$\beta$</sup>  resonances in the 29.0–30.0 ppm spectral window, which are highly supportive of the presence of free thiol moieties (Figure 2D). The directly bonded <sup>1</sup>H <sup>$\beta$</sup>  resonances for all three Cys residues support a reduced environment (free thiol state) for these <sup>13</sup>C <sup>$\beta$</sup>  resonances as observed in 2D <sup>1</sup>H–<sup>1</sup>H TOCSY and NOESY spectra (Figure 2A and Figure 2D). Interestingly, no <sup>13</sup>C <sup>$\beta$</sup>  resonances were observed for the oxidized conformation, which suggests that the single reduced conformational (free thiol) state may be more stable, while the two oxidized conformations may be interconverting on the NMR time scale, which we believe may result in exchange broadening.<sup>15</sup>

In Figure 2B and Figure 2C, some of the <sup>1</sup>H<sup>N</sup>–<sup>1</sup>H <sup>$\beta$</sup>  crosspeaks in the 2D TOCSY spectrum are not seen for these minor (disulfide) conformations. This is like the result of insufficiencies in the through bond magnetization transfer process, which may have occurred in this relatively fast interconverting oxidized state.

MALDI-TOF mass spectrometry performed on KR A1–15 NMR samples in the absence of DTT identified the presence

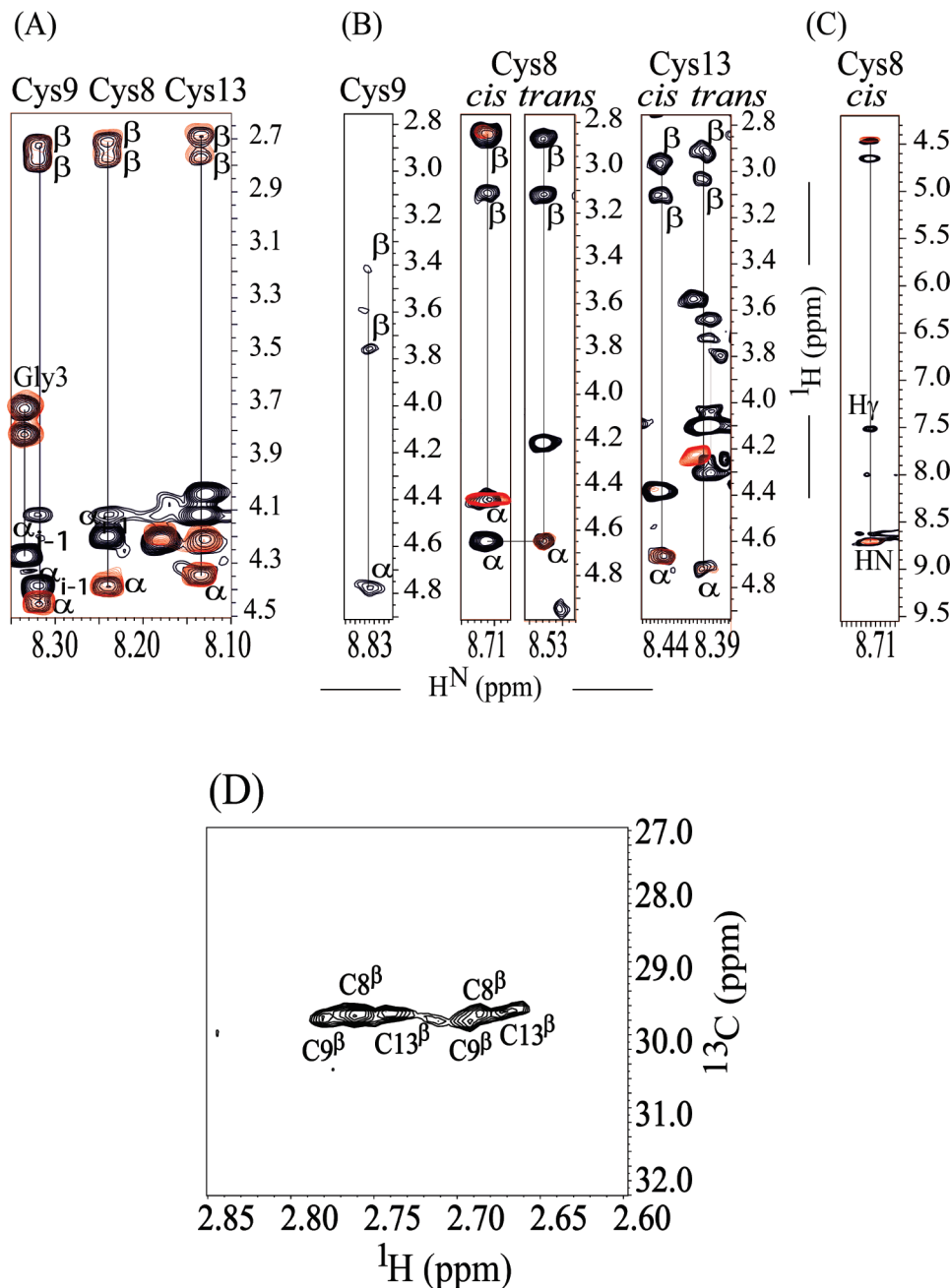


**Figure 2.** Overlay of Strip-plots from 2D  $^1\text{H}$ - $^1\text{H}$  NOESY ( $\tau_m = 300$  ms) (colored black), and 2D  $^1\text{H}$ - $^1\text{H}$  TOCSY (spin lock = 70 ms) (colored red) of KR A1-15, showing redox spin systems for all three Cys residues. (A) Reduced state chemical shifts. (B) Oxidized state chemical shifts in *cis* and *trans* conformations. (C) *Cis* conformer of Cys8, showing a sulfhydryl proton chemical shift at 7.52 ppm. (D) 2D  $^1\text{H}$ - $^{13}\text{C}$  HSQC: characteristic  $^{13}\text{C}^\beta$  of all three Cys are seen in reduced conformations (all data were acquired in the absence of DTT). NMR data were acquired at 288 K with the KR A1-15 peptide in 80% DMSO- $d_6$ /20%  $\text{H}_2\text{O}$ , pH 5.5, at a concentration of 2.16 mM, with a Bruker Avance 600 MHz spectrometer.

of monomer/dimer peaks in a ratio of  $\sim 1:2$  using the peak intensity of the representative conformations. These data further support that the reduced and oxidized conformational states are in equilibrium (Figure S4A, Supporting Information). In another sample containing 25 mM DTT, we only see monomeric (free thiol) KR A1-15 with no dimer peak (intermolecular disulfide bond formation) observed (Figure S4B, Supporting Information). These data are in good agreement with the functional observations that clearly illustrate approximately a 2-fold increase in T-cell recognition in the presence of 25 mM DTT (Figure S1, Supporting Information).

The two oxidized isomeric states of Cys8 and Cys13 were designated as *cis* and *trans* conformations. This discrimination

was based on the observation of a unique  $^1\text{H}^\text{N}$ - $^1\text{H}^\alpha$  intermolecular NOE between the two conformers of Cys8 that we have identified in a *cis:trans* ratio of 55%:45% (Figure 2B). A similar *cis:trans* Cys residue equilibrium [ratio of 0.7:0.3 ( $\pm 0.05$ )] has been reported previously in a NMR study of a heptapeptide comprised of vicinal cysteine residues.<sup>17</sup> The single oxidized state of Cys9 is characterized by a  $^1\text{H}^\beta$  crosspeak that is shifted downfield (with respect to the  $^1\text{H}^\beta$  resonance chemical shifts for Cys8 and Cys13) to 3.76 ppm (Figure 2B). The chemical shift of this downfield resonance is the result of the unique local environment that is sampled by this Cys residue and is consistent with previous studies of insulin peptides in an oxidizing environment [Table S1C, Supporting Information].

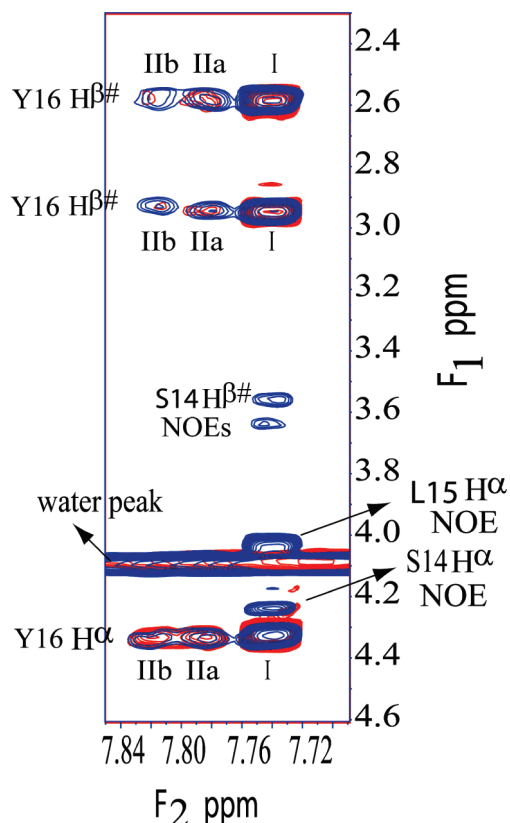


**Figure 3.** Overlay of contour plots from 2D  $^1\text{H}$ – $^1\text{H}$  NOESY ( $\tau_m = 300$  ms) (colored blue) and 2D  $^1\text{H}$ – $^1\text{H}$  TOCSY (spin lock = 70 ms) (colored red) shows three observed conformations of Tyr16 (the spin system for the major conformation is represented by I, and the two minor conformations, with respective population ratio of ~55:45, are represented by IIa and IIb). The population ratio between Tyr16 minor conformations in IIa and IIb states is similar as observed for two minor conformations of Cys8 and Cys13. Degenerate methylene proton chemical shifts are shown by  $\text{H}^{\beta\#}$ .

Interestingly, our 2D  $^1\text{H}$ – $^1\text{H}$  NOESY data also allowed us to identify the presence of a sulfhydryl proton ( $^1\text{H}^\gamma$ ) for the oxidized *cis* conformation of Cys8 at 7.52 ppm (Figure 2C). These data may suggest that Cys8 possibly participates in a mixed disulfide conformation ( $-\text{S}-\text{SH}$ ). A similar observation of the  $^1\text{H}^\gamma$  chemical shift (7.6 ppm) has been reported for Cys14 in *E. coli* glutaredoxin-3, a residue that was functionally important.<sup>18</sup>

Furthermore,  $^1\text{H}$ – $^1\text{H}$  homonuclear data (in the absence of DTT) also identified the presence of alternative amide spin systems for Ser14 and Tyr16, which are likely due to slow exchange properties of these amide protons and/or the redox nature of Cys residues (Cys 8, 9, and 13). The population ratio of major vs minor conformations for Ser14 and Tyr16 is analogous to that observed for the Cys residues (Figure 3). These data suggest that Ser14 and Tyr16 are in close proximity and thus sterically constrained by the redox state of these Cys residues.

The complete assignment of the 2D  $^1\text{H}$ – $^1\text{H}$  NOESY data (in the absence of DTT) in the oxidized state aided in our characterization of the multiple redox states of the KR A1–15 peptide. These data identified three weak NOEs between  $\text{Cys8H}^\beta$ – $\text{Cys13H}^\alpha$ ,  $\text{Cys8H}^\alpha$ – $\text{Cys13H}^\beta$ , and  $\text{Cys8H}^\beta$ – $\text{Cys13H}^\beta$  that support the presence of a disulfide bond between Cys8–Cys13. No such NOEs were observed for Cys9. These data propose that Cys9 may also be involved in forming an intermolecular disulfide bond between two KR A1–15 mol-

**TABLE 1: Comparison of Experimental (NMR) and Computational (Quantum Chemical) Results of  $^1\text{H}$  NMR Shifts<sup>a</sup> (ppm)**

		exptl	range	non-HB	HB
$\text{H}-\text{C}^\beta$	Cys–SH	2.68–2.78	0.10	2.54	2.59
	Cys–SHS–Cys	2.86–3.12	0.26	2.76	2.80
	Cys–SS–Cys	2.88–3.76	0.88	2.94	3.00
$\text{H}-\text{C}^\alpha$	Cys–SH	4.32–4.43	0.11	4.29	4.38
	Cys–SHS–Cys	4.47–4.66	0.19	4.55	4.64
	Cys–SS–Cys	4.65–4.78	0.13	4.67	4.76
$\text{H}-\text{N}$	Cys–SH	8.13–8.32	0.19	6.90	8.27
	Cys–SHS–Cys	8.44–8.71	0.27	6.42	8.47
	Cys–SS–Cys	8.39–8.83	0.44	6.98	8.67

<sup>a</sup> Non-HB calculations are those for Cys–SH, Cys–SS–Cys, and Cys–SHS–Cys alone, while HB calculations incorporate the backbone hydrogen bonding moiety to NH to simulate the protein backbone. All calculations here include the general effect of the bulk protein environment.

ecules, which may account for the faster thiol–disulfide interconversion rate that is observed in our data. We believe this may also explain the observed line broadening for the single oxidized spin system of Cys9 (Figure 2B). The disulfide arrangement found in KR A1–15 is similar to that in native human insulin molecule (Figure 1).<sup>19,20</sup>

To date, no prior theoretical investigations have been performed to evaluate the role and importance of Cys proton NMR chemical shifts as redox fingerprints in biomolecules. To further probe the redox state-dependent conformational flux observed for KR A1–15, we performed a number of quantum chemical calculations using state-of-the-art methods<sup>14</sup> (see Supporting Information for details). The theoretical investigations were used to evaluate if the observed NMR chemical shifts could be used to predict the unique redox state of the Cys residues in this peptide and possibly translate to other peptide systems. The computational results (*vide infra*) confirmed the presence of both a reduced and oxidized state for the KR A1–15 peptide and predicted the chemical shift for the highly unique thiol observed in our experimental NMR data (experimental, 7.52 ppm; calcd, 7.50 ppm). The experimental chemical shift range for each of the Cys protons ( $^1\text{H}^\alpha$ ,  $^1\text{H}^\beta$ , and  $^1\text{H}^\gamma$ ) in each of the unique redox states differs modestly (ca. 0.1–0.3 ppm, see Table 1). These data suggest that the observed NMR data result from local effects on the Cys residues alone and provide a basis for using computationally derived molecular models comprised of Cys–SH, Cys–SS–Cys, and Cys–SHS–Cys to represent the reduced, oxidized, and mixed redox states of the insulin A-chain epitope, respectively.

The first set of non-hydrogen bond (non-HB) calculations was performed on models outlined above in the absence of backbone HB partners to evaluate if the oxidation states of the Cys residues alone can reproduce the experimental trend observed: an incremental increase in chemical shift values for the proton(s) in the Cys residues in the order of Cys–SH < Cys–SHS–Cys < Cys–SS–Cys, (Table 1). Interestingly, for both the  $\text{C}^\alpha$  and  $\text{C}^\beta$  protons ( $^1\text{H}^\alpha$  and  $^1\text{H}^\beta$ ), the predicted NMR chemical shift data are in excellent agreement with the theoretically derived data (Figure S5, Supporting Information, and Table 1). The linear agreement between the calculated quantum chemical values and the average experimentally observed values for each conformation is represented by a correlation coefficient of  $R^2 = 0.998$  (standard deviation of 0.05 ppm) (Figure S5, Supporting Information, and Table 1). These results support that the observed chemical shift trend for  $^1\text{H}^\alpha$  and  $^1\text{H}^\beta$  can be ascribed to the different Cys oxidation states present in the three



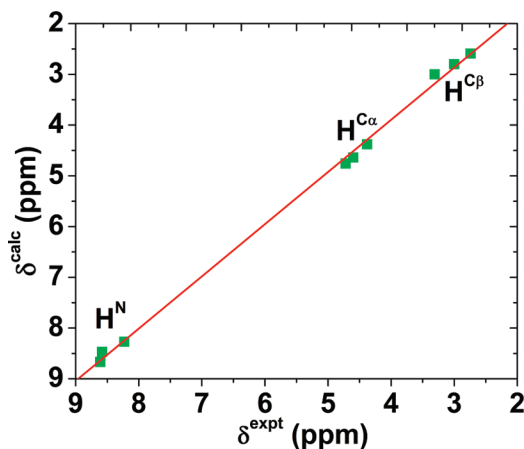


**Figure 4.** Correlation plot between the experimental and computational results for  $^1\text{H}^{\alpha}$ ,  $^1\text{H}^{\beta}$ , and  $^1\text{H}^{\text{N}}$  of reduced, oxidized, and mixed forms of Cys residues in KR A1–15.

conformations. However, the predicted amide proton ( $^1\text{H}^{\text{N}}$ ) NMR chemical shift data support a different trend, which we believe can be attributed to differences in the distance between the  $^1\text{H}^{\alpha}$  and  $^1\text{H}^{\beta}$  protons and the backbone  $^1\text{H}^{\text{N}}$  versus the sulfur atom involved in the respective redox state. Given that oxidized sulfur atoms are electron deficient and thus attract electrons from surrounding atoms, this reduces the electron density around these atoms and results in decreased chemical shielding and increased NMR chemical shifts as we have observed experimentally.

Given the discrepancy of  $\sim 2$  ppm between our experimentally observed and theoretically predicted  $^1\text{H}^{\text{N}}$  chemical shifts using the non-HB calculations, we carried out a second set of calculations that included a HB partner for each of the  $^1\text{H}^{\text{N}}$  protons (see Supporting Information for details). The predicted  $^1\text{H}^{\text{N}}$  NMR chemical shifts for the reduced, mixed, and oxidized states are 8.27, 8.47, and 8.67 ppm, respectively, which correlate well with the average experimental values of 8.23, 8.57, and 8.58 ppm, respectively (Figure 4 and Table 1). It is also interesting to note that the precision of the predicted  $^1\text{H}$  NMR chemical shifts of  $^1\text{H}^{\alpha}$  and  $^1\text{H}^{\beta}$  protons was also improved. These proton chemical shifts appear to be independent of the HB distances implemented into our theoretical calculations, which is consistent with their distal proximity to the HB region compared the  $^1\text{H}^{\text{N}}$  protons. As illustrated in Figure 4, there is a significant linear correlation ( $R^2 = 0.998$ ) between our experimentally observed and theoretically derived values with a standard deviation of 0.11 ppm or 1.9% of the experimental  $^1\text{H}$  NMR shift range observed for KR A1–15.

Taken together, our computational data support the presence of three redox states for the Cys residues in the human insulin A-chain epitope, which we have identified in our experimental NMR studies. Each of these redox states can be characterized by unique chemical shift data. In addition, these calculations support that the observed trend for the  $^1\text{H}^{\alpha}$  and  $^1\text{H}^{\beta}$  chemical shifts,  $\text{Cys-SH} < \text{Cys-SHS} < \text{Cys-SS-Cys}$ , which we believe can be attributed to the electronic effect of the Cys residue at each redox state (Table 1). However, we believe that the observed trend for the  $^1\text{H}^{\text{N}}$  chemical shifts is dependent on both the Cys redox state as well as the relevant HB network within the peptide structure.

In Figure S4A (Supporting Information), the relative signal/noise (S/N) ratio of the peak heights in the MALDI spectrum was used to estimate the monomer:dimer ratio. The peptide, in its dimer conformation, is comprised of two molecules, which may be interdisulfide linked via Cys9 in each peptide, while

the monomer peak height is representative of a single molecule. The increased peak intensity of the dimer conformation may additionally be due to the presence of some free thiol population of Cys 8 and Cys13 in it, if the formation of the dimer has taken place via interdisulfide bond formation (Cys9–Cys9) between two KR A1–15 peptide monomers. Importantly, one has to be cautious when comparing MS data from a plate spotted dried peptide sample possessing a fixed molecular composition at the time of the laser shot and NMR data that represent the presence of multiple, dynamic conformations that are sampled simultaneously on the NMR time scale.

The observation of multiple redox dependent states for the Cys residues of KR A1–15 is similar to those previously described for human serum albumin (HSA), in which Cys34 of HSA was observed to be predominantly in a free sulfhydryl conformation (70–80%) with the remaining Cys34 conformations representative of an oxidized and mixed disulfide isomeric conformation.<sup>21</sup>

The occurrence of multiple states in human insulin has been reported by others previously.<sup>22–24</sup> In a NMR study of the human insulin B-chain, Cys7 was present in multiple unique conformations including a major conformation (>90%) and minor conformations (accounting for <10%).<sup>24</sup> Similarly, two different conformations were observed for A-chain and B-chain residues in a NMR study of mutant human insulin.<sup>23</sup> However, our work provides the first atomic level evidence of the coexistence of the Cys reduced, oxidized, and a mixed disulfide ( $-\text{S}-\text{SH}$ ) conformations, which we believe are important redox-dependent conformations responsible for regulating the activity of this peptide and/or its targets.

The observation of a mixed disulfide conformer may represent a redox state that is short-lived on the NMR time scale when one considers the signal intensity of the  $^1\text{H}^{\gamma}$  crosspeak versus the crosspeak intensities for the reduced and oxidized conformational states. However, the emergence of the  $^1\text{H}^{\gamma}$  chemical shift may also represent the presence of a thiolate–thiol hydrogen bond pair formed between the Cys8 thiolate and the Cys13 thiol which are the residues responsible for the formation of the disulfide bond, a hypothesis that is supported by our NOESY data. Interestingly, a  $^1\text{H}^{\gamma}$  proton was observed in HSA that does indeed exist in plasma in the mixed disulfide conformation with other redox states.<sup>21</sup> To date, there are 89 reports of this unique thiol ( $^1\text{H}^{\gamma}$ ) chemical shift in the BMRB chemical shift database: (<http://www.bmrwisc.edu>). This proton has been assigned chemical shift values between 0.25 and 10.7 ppm depending upon the local protein environment. Indeed, our quantum chemical calculations support that different local environments affect the strength and/or distance between the two sulfurs of the thiolate–thiol hydrogen bonding interaction ( $\text{SH}\cdots\text{S}$ ) in the mixed disulfide state. Our calculations identify that the strongest  $\text{SH}\cdots\text{S}$  interaction has a predicted thiol proton shift of 11.13 ppm, which is very close to the experimental upper bound of 10.7 ppm reported in BMRB. This occurs in the fully optimized Cys–SHS–Cys model with no restraints, in which the distance separating the two sulfur atoms is 3.54 Å. However, when the two-sulfur distance is increased due to a specific protein environment, the reduced  $\text{SH}\cdots\text{S}$  interaction shifts this resonance upfield. Calculations were performed at various  $\text{S}(\text{H})\cdots\text{S}$  distances, and we determined that when this sulfur–sulfur distance is elongated by 0.35 Å the predicted thiol proton shift in the HB calculation of the mixed conformation is 7.50 ppm, which is in excellent agreement with our experimental observation of 7.52 ppm. Therefore, this proton shift is also a sensitive probe of the local redox

environment of the protein. In contrast to the established distance dependence for the thiol proton shifts, the C $^{\alpha}$ , C $^{\beta}$ , and amide proton shifts are only modestly affected ( $\leq 0.1$  ppm), which is within the computational error margin.

Mannering et al. have previously reported that T cell clone recognition of the KR A1–13 peptide required the presence of a vicinal disulfide bond between Cys6–Cys7.<sup>4b</sup> The disulfide bond arrangement they proposed was identified in a variant of the peptide in which the third Cys was mutated to a serine (Figure 1).<sup>4b</sup> In our present study of the KR A1–15 peptide that is comprised of all three Cys residues, our NOESY data support the presence of Cys8–Cys13 disulfide bond arrangement within oxidized state conformation, which is similar to that found in native insulin (Cys6–Cys11 disulfide pattern in native insulin) and do not observe the vicinal disulfide (Figure 1). In addition, T cell clones were generated from the periphery of a DR4+ new onset type 1 diabetes subject using single-cell sorting to identify those T cells that proliferated in response to recombinant human pro-insulin using a sensitive CSFE assay. These studies confirmed that these clones responded to the insulin KR A1–13 peptide and that this was a naturally processed epitope.<sup>4b</sup> During antigen processing, proteins are cleaved into linear peptides, 12–16 amino acids in length, by an array of proteases and modifying enzymes in the acidic lysosome of which there is differential expression and function among individual subjects, and then ultimately loaded into the groove of Class II proteins.<sup>4c,26–29</sup> The conformational flux of the insulin A-chain peptide(s) and how they are presented by the Class II cell surface protein can influence the T cell response to the autoantigenic protein.

It is worth noting that in previous NMR studies of a human insulin A-chain analogue (C7S, C20S), carried out in 100% DMSO, a single conformation was observed,<sup>25</sup> while studies carried out with a mutant human insulin in aqueous buffer reported the presence of at least two conformations.<sup>23,24</sup> These studies provide further support that the redox-dependent conformational states observed for the KR A1–15 peptide are intrinsic properties of the insulin A-chain.

## Conclusions

We have investigated the A-chain human insulin peptide, KR A1–15, which has reactivity with the T cell clone Ba.14 in a chemically reduced environment. NMR and mass spectroscopy coupled with quantum computational studies support the presence of three Cys redox states that are chemically distinct. Efforts are underway to determine the solution NMR structure of this insulin epitope in a reduced/active chemical environment. The observed Cys conformers and the redox-dependent thiol–disulfide exchange, which we believe is responsible for modulating T cell recognition and/or Class II MHC interactions by this insulin peptide in diabetes mellitus, may serve as a novel redox-dependent regulation mechanism that may be applicable to other proteins that are modulated by Cys redox chemistry.

**Acknowledgment.** The authors acknowledge James Sudmeier (Tufts NMR Center, Boston, MA) for helpful discussion during NMR data acquisition, Simon Dillon for MS data acquisition and discussions (BIDMC Proteomics Center, Boston, MA), the computing facilities in the Mississippi Center for Supercomputing Research, and the USM Vislab. This work was supported by an Atorvastatin Research Award (A.C.R.), by the JDRFI grant (S.C.K.), and P01 AI045757, U19 AI046130, U19 AI070352, P01 AI039671, and a Jacob Javits Merit Award (NS2427) from the NINDS (D.A.H.), and by the NSF EPSCoR grant OIA-0556308 (Y.Z.) and NIH grant GM-085774 (Y.Z.).

**Supporting Information Available:** Experimental details of T-cell, NMR experiments with  $^1\text{H}$ ,  $^{13}\text{C}$  chemical shift values, and computational information (Tables S1–S4 and Figures S1–S5). This material is available free of charge via the Internet at <http://pubs.acs.org>.

## References and Notes

- (1) (a) Atkinson, M. A.; Maclaren, N. K. *N. Engl. J. Med.* **1994**, *331*, 1428–1436. (b) Di Lorenzo, T. P.; Peakman, M.; Roep, B. O. *Clin. Exp. Immunol.* **2007**, *148*, 1–16. (c) Eisenbarth, G. S. *N. Engl. J. Med.* **1986**, *314*, 1360–1368.
- (2) (a) Brown, H.; Sanger, F.; Kitai, R. *Biochem. J.* **1955**, *60*, 556–565. (b) Ryle, A. P.; Sanger, F.; Smith, L. F.; Kitai, R. *Biochem. J.* **1955**, *60*, 541–556.
- (3) (a) Tang, J.-G.; Wang, C. C.; Tsou, C. L. *Biochem. J.* **1998**, *255*, 451–455. (b) Wang, C. C.; Tsou, C.-L. *Trends Biochem. Sci.* **1991**, *16*, 279–281.
- (4) (a) Kent, S. C.; Chen, Y.; Bregoli, L.; Clemmings, S. M.; Kenyon, N. S.; Ricordi, C.; Hering, B. J.; Hafler, D. A. *Nature* **2005**, *435*, 224–228. (b) Mannering, S. I.; Harrison, L. C.; Williamson, N. A.; Morris, J. S.; Thearle, D. J.; Pensén, K. P.; Kay, T. W. H.; Rossjohn, J.; Falk, B. A.; Nepom, G. T.; Purcell, A. W. *J. Exp. Med.* **2005**, *202*, 1191–1197. (c) Bryant, P.; Ploegh, H. *Curr. Opin. Immunol.* **2004**, *16*, 96–102. (d) van Niel, G.; Wubbolts, R.; Stoorvogel, W. *Curr. Opin. Cell Biol.* **2008**, *20*, 437–444. (f) Marttila, J.; Huttunen, S.; Vaarala, O.; Suzuki, K.; Elliott, J. F.; Närvänen, A.; Knip, M.; Simell, O.; Ilonen, J. *J. Autoimmun.* **2008**, *31*, 142–148.
- (5) Jensen, P. E. *J. Exp. Med.* **1991**, *174*, 1121–1130.
- (6) Sharma, A. K.; Zhou, G.-P.; Kupferman, J.; Surks, H.; Christensen, E.; Chou, J. J.; Mendelsohn, M.; Rigby, A. C. *J. Biol. Chem.* **2008**, *283*, 32860–32869.
- (7) (a) Bax, A.; Davis, D. G. *J. Magn. Reson. A* **1985**, *63*, 207–213. (b) Piotto, M.; Saudek, V.; Sklenar, V. *J. Biomol. NMR* **1992**, *2*, 661–665. (c) Sklenar, V.; Piotto, M.; Leppik, R.; Saudek, V. *J. Magn. Reson. A* **1993**, *102*, 241–245.
- (8) (a) Palmer, A. G., III; Cavanagh, J.; Wright, P. E.; Rance, M. *J. Magn. Reson.* **1991**, *93*, 151–170. (b) Vuister, G. W.; Bax, A. *J. Magn. Reson.* **1992**, *98*, 428–435.
- (9) Delaglio, F.; Grzesiek, S.; Vuister, G. W.; Zhu, G.; Pfeifer, J.; Bax, A. *J. Biomol. NMR* **1995**, *6*, 277–293.
- (10) (a) Kraulis, P. J. *J. Magn. Reson.* **1989**, *84*, 627–633. (b) Kraulis, P. J.; Domaille, P. J.; Campbell-Burk, S. L.; van Aken, T.; Laue, E. D. *Biochemistry* **1994**, *33*, 3515–3531.
- (11) Becke, A. D. *J. Chem. Phys.* **1993**, *98*, 5648–5652.
- (12) Ditchfield, R. *Mol. Phys.* **1974**, *27*, 789–807.
- (13) Frisch, M. J.; Trucks, G. W.; Schlegel, H. B.; Scuseria, G. E.; Robb, M. A.; Cheeseman, J. R.; Montgomery, J. A., Jr.; Vreven, T.; Kudin, K. N.; Burant, J. C.; Millam, J. M.; Iyengar, S. S.; Tomasi, J.; Barone, V.; Mennucci, B.; Cossi, M.; Scalmani, G.; Rega, N.; Petersson, G. A.; Nakatsuji, H.; Hada, M.; Ehara, M.; Toyota, K.; Fukuda, R.; Hasegawa, J.; Ishida, M.; Nakajima, T.; Honda, Y.; Kitao, O.; Nakai, H.; Klene, M. Li, X.; Knox, J. E.; Hratchian, H. P.; Cross, J. B.; Bakken, V.; Adamo, C.; Jaramillo, J.; Gomper, R.; Stratmann, R. E.; Yazyev, O.; Austin, A. J.; Cammi, R.; Pomelli, C.; Ochterski, J. W.; Ayala, P. Y.; Morokuma, K.; Voth, G. A.; Salvador, P.; Dannenberg, J. J.; Zakrzewski, V. G.; Dapprich, S.; Daniels, A. D.; Strain, M. C.; Farkas, O.; Malick, D. K.; Rabuck, A. D.; Raghavachari, K.; Foresman, J. B.; Ortiz, J. V.; Cui, Q.; Baboul, A. G.; Clifford, S.; Cioslowski, J.; Stefanov, B. B.; Liu, G.; Liashenko, A.; Piskorz, P.; Komaromi, I.; Martin, R. L.; Fox, D. J.; Keith, T.; Al-Laham, M. A.; Peng, C. Y.; Nanayakkara, A.; Challacombe, M.; Gill, P. M. W.; Johnson, B.; Chen, W.; Wong, M. W.; Gonzalez, C.; Pople, J. A. *Gaussian 03*, revision D.01; Gaussian, Inc.: Wallingford, CT, 2004.
- (14) (a) Mukkamala, D.; Zhang, Y.; Oldfield, E. *J. Am. Chem. Soc.* **2007**, *129*, 7385–7392. (b) Cheng, F.; Sun, H. H.; Zhang, Y.; Mukkamala, D.; Oldfield, E. *J. Am. Chem. Soc.* **2005**, *127*, 12544–12554.
- (15) Wuthrich, K. *NMR of proteins and Nucleic Acids*; John Wiley and Sons: New York, 1986.
- (16) (a) Wishart, D. S.; Bigam, C. G.; Holm, A.; Hodges, R. G.; Sykes, B. D. *J. Biomol. NMR* **1995**, *5*, 67–81. (b) Wishart, D. S.; Case, D. A. *Methods Enzymol.* **2001**, *338*, 3–34.
- (17) Sukumaran, D. K.; Prorok, M.; Lawrence, D. S. *J. Am. Chem. Soc.* **1991**, *113*, 706–707.
- (18) Nordstrand, K.; Aslund, F.; Meunier, S.; Holmgren, A.; Otting, G.; Berndt, K. D. *FEBS Lett.* **1999**, *449*, 196–200.
- (19) Blundell, T. L.; Dobson, G. G.; Hodgkin, D. C.; Mercola, D. A. *Adv. Protein Chem.* **1972**, *26*, 279–402.
- (20) Cutfield, J. F.; Cutfield, S. M.; Dobson, E. J.; Dobson, G. G.; Emdin, S. O.; Reynolds, C. D. *J. Mol. Biol.* **1979**, *132*, 85–100.
- (21) Oettl, K.; Stauber, R. E. *Br. J. Pharmacol.* **2007**, *151*, 580–590.
- (22) Kline, A. D.; Richard, M. J., Jr. *Biochemistry* **1990**, *29*, 2906–2913.

- (23) Keller, D.; Clausen, R.; Josefsen, K.; Led, J. J. *Biochemistry* **2001**, *40*, 10732–10740.
- (24) Hua, Q.-X.; Jia, W.; Frank, B. H.; Phillips, N. F. B.; Weiss, M. A. *Biochemistry* **2002**, *41*, 14700–14715.
- (25) Flem, G. L.; Dupradeau, F.-Y.; Pujol, J.-P.; Monti, J.-P.; Bogdanowicz, P. *Bioorg. Med. Chem.* **2002**, *10*, 2111–2117.
- (26) Brown, J. H.; Jardetzky, T. S.; Gorga, J. C.; Stern, L. J.; Urban, R. G.; Strominger, J. L.; Wiley, D. C. *Nature* **1993**, *364*, 33–39.
- (27) Vyas, J. M.; Van der Veen, A. G.; Ploegh, H. L. *Nat. Rev. Immunol.* **2008**, *8*, 607–618.
- (28) Lennon-Duménil, A. M.; Bakker, A. H.; Wolf-Bryant, P.; Ploegh, H. L.; Lagaudrière-Gesbert, C. *Curr. Opin. Immunol.* **2002**, *14*, 15–21.
- (29) Costantino, C. M.; Hang, H. C.; Kent, S. C.; D. A. Hafler, D. A.; Ploegh, H. L. *J. Immunol.* **2008**, *180*, 2876–85.

JP908729H